参　考　文　献

1)Kaper JB, Nataro JP and Mobley HL. Pathogenic *Escherichia coli*. Nat Rev Microbiol 2004 ; 2 : 123-40.

2)Caprioli A, Morabito S, Brugere H, *et al.* Enterohaemorrhagic *Escherichia coli* : emerging issues on virulence and modes of transmission. Vet Res 2005 ; 36 : 289-311.

3)Hayashi T, Makino K, Ohnishi M, *et al.* Complete genome sequence of enterohemorrhagic *Escherichia coli* O157 : H7 and genomic comparison with a laboratory strain K-12. DNA Res 2001 ; 8 : 11-22.

4)Perna NT, Plunkett G, 3rd, Burland V, *et al.* Genome sequence of enterohaemorrhagic *Escherichia coli* O157 : H7. Nature 2001 ; 409 : 529-33.

5)Tobe T, Beatson SA, Taniguchi H, *et al.* An extensive repertoire of type III secretion effectors in *Escherichia coli* O157 and the role of lambdoid phages in their dissemination. Proc Natl Acad Sci USA 2006 ; 103 : 14941-6.

6)戸邊　亨. 病原性大腸菌および赤痢菌における環境応答による病原性発現調節. 日本細菌学雑誌 2007 ; 62 : 337-46.

7)Reid SD, Herbelin CJ, Bumbaugh AC, *et al.* Parallel evolution of virulence in pathogenic *Escherichia coli*. Nature 2000 ; 406 : 64-7.

8)Ogura Y, Ooka T, Iguchi A, *et al.* Comparative genomics reveal the mechanism of the parallel evolution of O157 and non-O157 enterohemorrhagic *Escherichia coli*. Proc Natl Acad Sci USA 2009 ; 106 : 17939-44.

9)Ogura Y, Abe H, Katsura K, *et al.* Systematic identification and sequence analysis of the genomic islands of the enteropathogenic *Escherichia coli* strain B171-8 by the combined use of whole-genome PCR scanning and fosmid mapping. J Bacteriol 2008 ; 190 : 6948-60.

10)Iguchi A, Thomson NR, Ogura Y, *et al.* Complete genome sequence and comparative genome analysis of enteropathogenic *Escherichia coli* O127 : H6 strain E2348/69. J Bacteriol 2009 ; 191 : 347-54.

11)Feng PC, Monday SR, Lacher DW, *et al.* Genetic diversity among clonal lineages within *Escherichia coli* O157 : H7 stepwise evolutionary model. Emerg Infect Dis 2007 ; 13 : 1701-6.

12)Ogura Y, Kurokawa K, Ooka T, *et al.* Complexity of the genomic diversity in enterohemorrhagic *Escherichia coli* O157 revealed by the combinational use of the O157 Sakai OligoDNA microarray and the Whole Genome PCR scanning. DNA Res 2006 ; 13 : 3-14.

13)Ohnishi M, Terajima J, Kurokawa K, *et al.* Genomic diversity of enterohemorrhagic *Escherichia coli* O157 revealed by whole genome PCR scanning. Proc Natl Acad Sci USA 2002 ; 99 : 17043-8.

14)Ooka T, Ogura Y, Asadulghani M, *et al.* Inference of the impact of insertion sequence(IS)elements on bacterial genome diversification through analysis of small-size structural polymorphisms in *Escherichia coli* O157 genomes. Genome Res 2009 ; 19 : 1809-16.

15)Asadulghani M, Ogura Y, Ooka T, *et al.* The defective prophage pool of *Escherichia coli* O157 : prophage-prophage interactions potentiate horizontal transfer of virulence determinants. PLoS Pathog 2009 ; 5 : e1000408.

16)Kusumoto M, Ooka T, Nishiya Y, *et al.* Insertion sequence-excision enhancer removes transposable elements from bacterial genomes and induces various genomic deletions. Nat Commun 2011 ; 2 : 152.

17)Ooka T, Terajima J, Kusumoto M, *et al.* Development of a multiplex PCR-based rapid typing method for enterohemorrhagic *Escherichia coli* O157 strains. J Clin Microbiol 2009 ; 47 : 2888-94.

18)Manning SD, Motiwala AS, Springman AC, *et al.* Variation in virulence among clades of *Escherichia coli* O157 : H7 associated with disease outbreaks. Proc Natl Acad Sci USA 2008 ; 105 : 4868-73.

19)Shimizu T, Tsutsuki H, Matsumoto A, *et al.* The nitric oxide reductase of enterohaemorrhagic *Escherichia coli* plays an important role for the survival within macrophages. Mol Microbiol 2012 ; 85 : 492-512.

20)Boerlin P, McEwen SA, Boerlin-Petzold F, *et al.* Associations between virulence factors of Shiga toxin-producing *Escherichia coli* and disease in humans. J Clin Microbiol 1999 ; 37 : 497-503.

21)Kawano K, Okada M, Haga T, *et al.* Relationship between pathogenicity for humans and stx genotype in Shiga toxin-producing *Escherichia coli* serotype O157. Eur J Clin Microbiol Infect Dis 2008 ; 27 : 227-32.

22)Matano S, Inamura K, Konishi M, *et al.* Encephalopathy, disseminated intravascular coagulation, and hemolytic-uremic syndrome after infection with enterohemorrhagic *Escherichia coli* O111. J Infect Chemother 2012 ; 18 : 558-64.

23)Paton AW, Srimanote P, Woodrow MC, *et al.* Characterization of Saa, a novel autoagglutinating adhesin produced by locus of enterocyte effacement-negative Shiga-toxigenic *Escherichia coli* strains that are virulent for humans. Infect Immun 2001 ; 69 : 6999-7009.

24)Lu Y, Iyoda S, Satou H, *et al.* A new immunoglobulin-binding protein, EibG, is responsible for the chain-like adhesion phenotype of locus of enterocyte effacement-negative, shiga toxin-producing Escherichia coli. Infect Immun 2006 ; 74 : 5747-55.

25)Paton AW, Beddoe T, Thorpe CM, *et al.* AB5 subtilase cytotoxin inactivates the

endoplasmic reticulum chaperone BiP. Nature 2006 ; 443 : 548-52.
26) Wang H, Paton JC and Paton AW. Pathologic changes in mice induced by subtilase cytotoxin, a potent new *Escherichia coli* AB5 toxin that targets the endoplasmic reticulum. J Infect Dis 2007 ; 196 : 1093-101.
27) Brzuszkiewicz E, Thurmer A, Schuldes J, *et al.* Genome sequence analyses of two isolates from the recent *Escherichia coli* outbreak in Germany reveal the emergence of a new pathotype: Entero-Aggregative-Haemorrhagic *Escherichia coli* (EAHEC). Arch Microbiol 2011 ; 193 : 883-91.
28) Mellmann A, Harmsen D, Cummings CA, *et al.* Prospective genomic characterization of the German enterohemorrhagic *Escherichia coli* O104 : H4 outbreak by rapid next generation sequencing technology. PLoS One 2011 ; 6 : e22751.
29) Rasko DA, Webster DR, Sahl JW, *et al.* Origins of the *E. coli* strain causing an outbreak of hemolytic-uremic syndrome in Germany. N Engl J Med 2011 ; 365 : 709-17.
30) Touchon M, Hoede C, Tenaillon O, *et al.* Organised genome dynamics in the *Escherichia coli* species results in highly diverse adaptive paths. PLoS Genet 2009 ; 5 : e1000344.

特集　大腸菌O111による脳症

腸管出血性大腸菌O111の進化と病原性*

小椋義俊**,***／大岡唯祐***／林　哲也**,***

Key Words：evolution, genome, pathogenicity, Shiga toxin, type III secretion system

腸管出血性大腸菌とは

大腸菌*Escherichia coli*(*E. coli*)はヒトを含む多くの脊椎動物の腸内常在菌の一つであり，基本的には病原性はないか日和見感染を起こすのみである．しかし，病原性大腸菌と呼ばれる一部の菌株はヒトに対して明らかな病原性を示す．病原性大腸菌は，腸管感染症を起こすもの(下痢原性大腸菌，diarrheagenic *E. coli*：DEC)と腸管外感染症を起こすもの(extraintestinal pathogenic *E. coli*：ExPEC)に大別され，前者はさらに5ないしは6種類の病原型に分類され，それぞれが異なった病原性を有し臨床的にも疫学的にも異なった特徴を示す．後者も尿路病原性大腸菌(uropathogenic *E. coli*：UPEC)や新生児髄膜炎の起因菌などに分類される[1)2)]．同じ大腸菌の中に，このように多様な病原菌株が出現したメカニズムは，それぞれの病原型に特有な外来性の病原遺伝子セットの獲得によると考えられる[3)]．

下痢原性大腸菌の中で，先進諸国において特に問題となっているのが腸管出血性大腸菌(enterohemorrhagic *E. coli*：EHEC)である．その理由は，①感染力が強いために，多数の散発事例だけでなく，たびたび大規模な集団感染を起こすこと，②激しい腹痛と出血を伴う出血性大腸炎を起こすこと，③生死にかかわる重篤な合併症をひき起こし，先進諸国の医療レベルをもってしても，ある一定の割合で亡くなる患者が出ること，④保菌動物(主にウシ)などの腸管に相当な頻度で定着しており感染源となるが，症状を呈さないことがほとんどであり，感染源の排除は難しいこと，などである．

EHECとしては，O157の血清型を持つ菌株がもっとも有名であるが，ほかにもさまざまな血清型を持つEHECが存在し，本稿のテーマであるO111もそういったnon-O157 EHECの一つである．すべてのEHECに共通する特徴は，志賀毒素Shiga toxin(Stx)と呼ばれる強力な毒素を産生することである(Stxはベロ毒素とも呼ばれたが，現在はShiga toxinと呼ぶ方向で統一されつつある)．Stxの遺伝子はバクテリオファージ(細菌を宿主とするウイルス)が運んでおり，Stxファージの感染と染色体へのファージゲノムの挿入(溶原化してプロファージとなる)によってStx産生性が付与されている．

多様な腸管出血性大腸菌とその中でのO111の位置づけ

前述のように，EHECにはさまざまな血清型を

* Evolution and pathogenicity of enterohemorrhagic *Escherichia coli* O111.

** Yoshitoshi OGURA, Ph.D., ***Tadasuke OOKA, Ph.D. & Tetsuya HAYASHI, M.D., Ph.D.: 宮崎大学フロンティア科学実験総合センター環境生命科学分野，***医学部感染症学講座微生物学分野〔〒889-1692　宮崎県宮崎市清武町木原5200〕; Division of Bioenvironmental Science, Frontier Science Research Center and ***Division of Microbiology, Department of Infectious Diseases, Faculty of Medicine, University of Miyazaki, Miyazaki 889-1692, Japan.

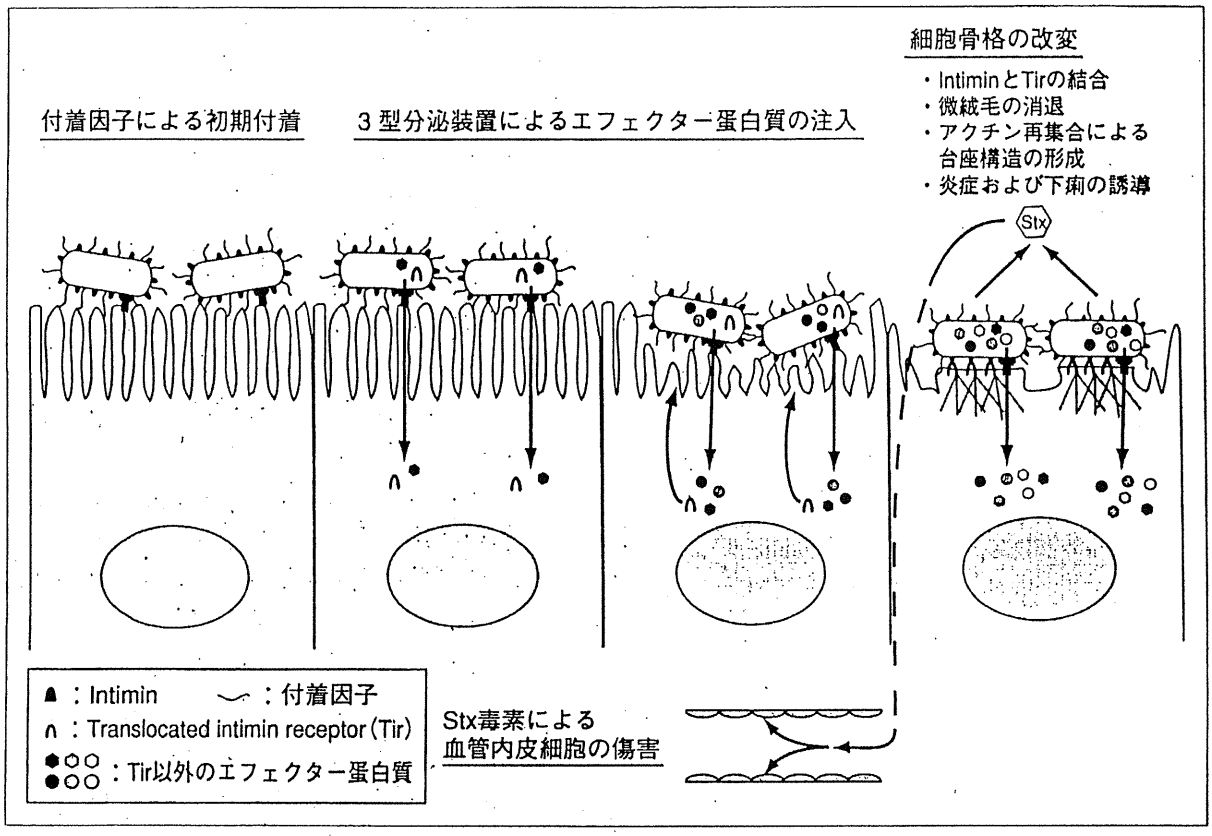

図1　EHECの感染過程とStx毒素の産生

もつ菌株が存在するが，大きく二つのグループ，典型的なもの(typical EHEC)と非典型的なもの(atypical EHEC)に分けて考えることが一般的である．また，Stx産生大腸菌全体をShiga toxin-producing *E. coli*(STEC)と呼ぶこともある．

1．典型的EHEC

典型的EHECは，locus for enterocyte effacement(LEE)と呼ばれるゲノム領域を有し，この領域には3型分泌系type III secretion system(T3SS)という蛋白質分泌装置，T3SSによって分泌される数種の蛋白質(エフェクターと呼ぶ)，インチミン(intimin)と呼ばれる細胞付着因子，遺伝子発現調節蛋白質などがコードされている．典型的EHECはこのT3SSを使ってエフェクター蛋白質を宿主細胞内に直接注入し，腸管上皮細胞の形態・機能を変化させる(図1)．特に重要なエフェクターはtranslocated intimin receptor(Tir)いう蛋白質であり，細胞内に注入されたTirは上皮細胞の細胞膜(腸管の内腔に面するapical surface)に移行し，細菌細胞の表層に存在するインチミンと結合する．この時，Tirを起点としてアクチンの再重合が細胞膜直下で誘導されるため，微絨毛が消失し，細菌細胞が結合した細胞膜部分が台座状に盛り上がった特有の形態が生じる(attaching and effacing lesionの形成)．

LEE領域は腸管病原性大腸菌(enteropathogenic *E. coli*：EPEC：DECの一つでサルモネラ様の腸炎を起こす)にも存在するため，EPECと典型的EHECの腸管への付着と腸炎の誘導は同じような仕組みによるといえる．また，やや乱暴な表現ではあるが，典型的EHECはEPECとして進化した大腸菌にStxファージが感染することによって誕生したともいえる．ただし，後述するように典型的EHECの病原因子はStxとLEE領域がコードするT3SSだけではない．

典型的EHECの代表はO157であるが，典型的EHECにはO157以外の血清型をもつもの(non-O157 EHEC)も多数存在し，その中で比較的メジャーな血清型はO26, O111, O103などである．典型的EHECはいずれもO157と同様の病原性を有すると考えられているが，溶血性尿毒症症候群(hemolytic uremic syndrome：HUS)などを合併し重症化する頻度が比較的高いnon-O157 EHECとしては，O26, O111, O103, O121, O145があ

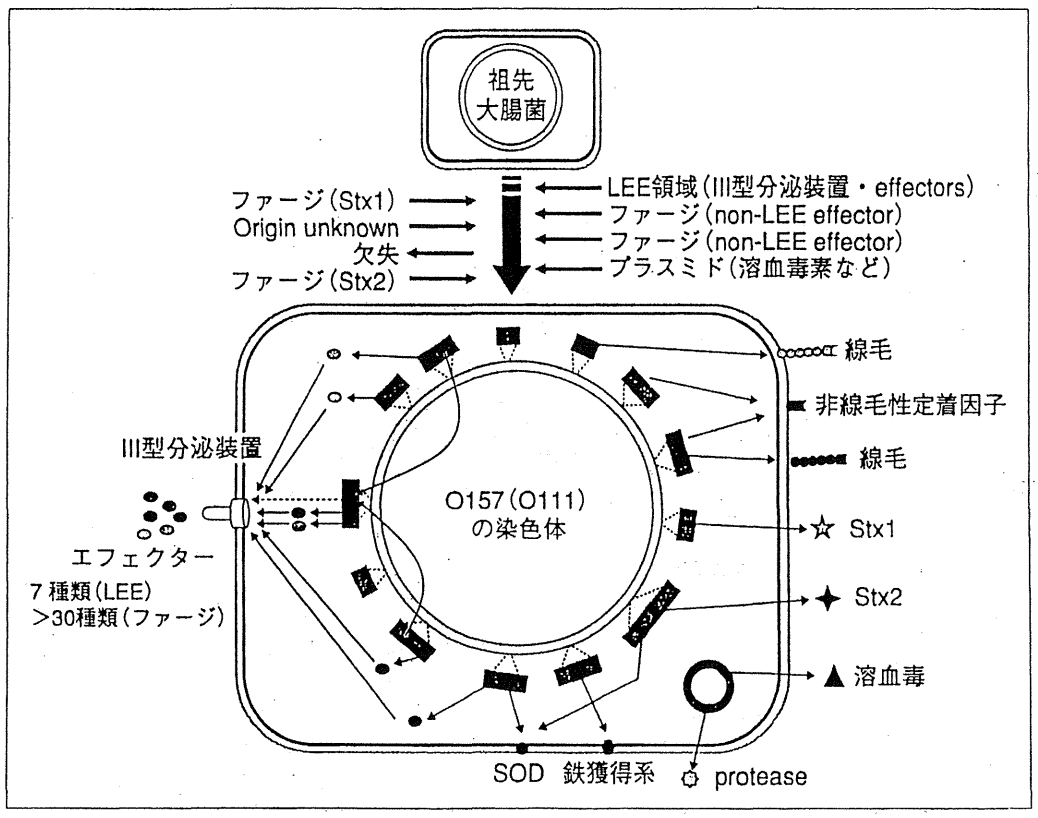

図2　バクテリオファージなどを介した外来性病原遺伝子の獲得によるO157とO111の進化のメカニズム(模式図)
この模式図はO157のゲノム解析から明らかになってきたO157の出現・進化の過程を示すために作成したものであるが，模式的にはO111の出現・進化の過程もまったく同じである．

げられる[4]．

2．非典型的EHECとO104：H4

Stxを産生するがLEE領域を保有しない大腸菌を一括りにして非典型的EHECという．LEE領域をもたないことから，腸管への付着と腸炎発症のメカニズムは典型的EHECの機構とは異なると考えられるが，その解析はほとんど進んでいない．非典型的EHECの代表はO113やO91などの血清型であるが，その他のマイナーな血清型も多数存在する．O113やO91などはヒトに対して確実な病原性を有し，出血性大腸炎やHUSなどの合併症もひき起こすこともある．しかし，その他のマイナーな血清型には単に*stx*遺伝子を有するだけの菌も含まれていると考えられ，病原性があるか否かがはっきりしないものが大部分である．

非典型的EHECの中で注目されるのは，2011年の5月，6月にヨーロッパで大規模な集団感染をひき起こしたO104：H4の血清型を持つ菌株である．この血清型のEHECは以前にも分離されたことがあるが[5]，きわめて稀な血清型であり，まったく注目されていなかった．しかし，今回の事例ではドイツを中心とする欧州各国で3,000人以上の患者が発生し，800人以上の重症患者と40人以上の死者が出た[6]．したがって，非典型的EHECも決して軽視してはならない．なお，今回のO104：H4菌株については，いくつかの研究機関とシーケンサー製造企業などが新型シーケンサーを用いてきわめて短時間で概要配列を決定し，しかも論文発表の前にインターネットなどを通じて公開し[7][8]，多くの研究者がその配列解析に参加した．その結果，非常に早い段階で，この菌株が腸管凝集性大腸菌(enteroaggregative *E. coli*：EAEC)と呼ばれるタイプの下痢原性大腸菌にStxをコードするファージが感染したものであることが明らかとなった[7][8]．

O111研究の現状

前項で述べたように，O111の血清型を持つEHECは，O157と同じようにLEE領域を持つ典

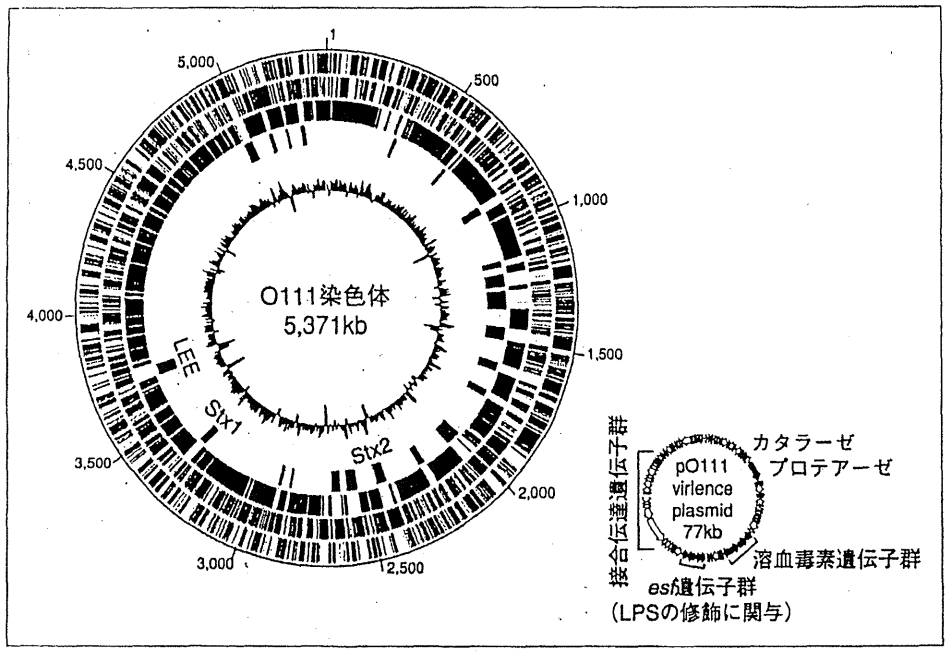

図3　O111の染色体とpO111ビルレンスプラスミドの構造

染色体のサークル図では，1番目と2番目のサークル上のバーはそれぞれDNA鎖(時計回りあるいは反時計回りの方向になる)にコードされている蛋白コード遺伝子を示し，3番目のサークル上のバーはO111の染色体上の全遺伝子のうちで非病原性大腸菌K-12株にも存在するものを表す．4番目のサークルにはファージあるいはファージ様遺伝因子を示し，5番目のサークルはDNA配列の塩基組成(GC含量)を示す．この図から，多数のファージとファージ様遺伝因子により多数の外来性遺伝子(したがって，K-12株には存在しない)が運び込まれていることがわかる．われわれがゲノム解読を行ったO111株には5種類のプラスミドが存在するが，その一つであるpO111ビルレンスプラスミドの構造を右に示す．なお，図には示さないが，このO111株の有する205 Kbのプラスミドは多剤耐性プラスミドであり，アンピシリン，カナマイシン，ストレプトマイシン，テトラサイクリン，サルファ剤，水銀に対する耐性遺伝子がコードされている．

型的なEHECの一つである．ただし，わが国での分離頻度はO157, O26に次いで3番目であり，EHEC全体の約4％を占めるにすぎない(O157が約70％，O26は約20％)．この傾向は世界的にも同じであり，O111は2番目にメジャーなnon-O157 EHECという位置づけになる．このため，ほとんどのEHECに関する研究はO157で行われてきた．これには，2001年という早い時期に大腸菌としては非病原性の実験室株であるK12株の次に，米国のグループによってO157 EDL933株(米国で1980年代に分離された菌株)[9]とわれわれのグループによってO157 Sakai株(1996年に大阪堺市で発生した大規模集団感染の原因菌株)[10]の全ゲノム配列が解読されたことも大きく関係しており，ゲノム情報が利用できるようになったことでO157を用いた研究が大きく前進した．

こういった状況から，O111 EHEC自体の病原性解析は非常に少ないのが実情である．しかし，2009年にわれわれのグループがO26およびO103とともにO111の全ゲノム配列の決定を行うことに成功し，O111が保有する病原遺伝子セットはO157のものと非常によく似ていることが判明した[11]．この結果は，O111の基本的な病原性メカニズムは，O157の全ゲノム情報やゲノム情報に基づいた世界各国の研究者によって展開されている多くの研究によって少しずつ明らかにされてきたO157の病原性メカニズムとよく似たものであることを意味する．したがって，次項では，O157での研究成果とO111のゲノム情報から推測しうるO111 EHECの出現と病原性メカニズムについて述べる．

腸管出血性大腸菌O111が出現した過程と病原性メカニズム

1．O111などの典型的なEHECが出現した過程

EHECだけでなく，各タイプの病原性大腸菌の

表1　O111 EHECのT3SSエフェクターレパートリー：O157, O26, EPECとの比較

	報告されている細胞内での機能または表現型	EHEC** O111	EHEC** O157	EHEC** O26	EPEC** (E2348/69株)
EspB*	輸送孔を形成，接着接合(adherens junction)の破壊，ミオシン結合による貪食阻害	1	1	1	1
EspF*	ミトコンドリアの破壊，NHE3の不活化，SGLT-1の不活化，タイトジャンクションの破壊，核の破壊，中間フィラメントの破壊，SNX9の活性化(膜のリモデリングを誘導)，N-WASPへの結合と活性化，PI3K依存性の貪食の阻害	1	1	1	1
EspG*	マイクロチュブールの破壊(ARF GTPase系の阻害，PAK系の刺激して膜輸送の阻害)	1	1	1	2
EspH*	Rho GTPase系の阻害，FCγR-を介した貪食を阻害，アクチン凝集(長さ)の亢進	1	1	1	1
EspJ	FCγR-およびCR3系を介したtrans-phagocytosisを阻害	1	1	1	1
EspK	不明	1	1	2	0
EspL	Annexin 2のF-actin bundling活性の阻害	2(1)	1	1	2(1)
EspM	RhoA GEF(ストレスファイバーの形成を誘導)	2	2	2	0
EspN	不明	1	1	1	0
EspO	不明	2	2	2	1(1)
EspV	細胞骨格の修飾	1(1)	1(1)	1(1)	0
EspW	不明	1	1	1	0
EspX	不明	1	1	1	0
EspZ*	β1-integrinとFAKの経路を刺激してアポトーシスと細胞毒性を阻害	1	1	1	1
Map*	Cdc42 GEF(一時的なfilopodia形成，ミトコンドリアの破壊，SGLT-1の不活化およびタイトジャンクションの破壊を誘導)	1	1	1	1
NleA/EspI	COPII依存的なERからの蛋白質輸送を阻害，タイトジャンクションの破壊	1	1	1(1)	1
NleB	TNF-が誘導するNF-κBの活性化を阻害	2	3(1)	1	3(1)
NleC	メタロプロテアーゼ〔p65(RelA)，c-Rel, p50, IκBを切断してNF-κB活性化を抑制〕	2	1	1	1
NleD	メタロプロテアーゼ(JNKを切断してAP-1の活性化を阻害)	0	1	0	1
NleE	IκB分解の阻害によるNF-κB活性化の抑制	2	1	1	2
NleF	不明	1(1)	1	1	1
NleG	U-box E3ユビキチンキナーゼ	11(3)	14(6)	14	1
NleH	Bax-inhibitor 1に結合(アポトーシスの抑制，RPS3を抑えてNF-κB系を阻害)	2	2	2	3(1)
TccP	N-WASPの自己抑制解除(台座形成の開始)	1	2(1)	1	0
Tir*	インチミンのレセプター(台座形成，Map依存性のfilopodia形成の抑制，SGLT-1の不活化)	1	1	1	1
Cif	NEDD8の脱アミド化を介したCRL活性の抑制〔p21とp27の蓄積とG(2)/G(1)cell cycle arrestの誘導〕	1(1)	0	1(1)	1(1)
Ibe	台座形成の亢進	1	0	2	0
OspG	Ser/Thrプロテインキナーゼ(phospho-IκBのユビキチン化・分解およびNF-κB活性化の阻害)	1	0	0	0
Total		44(7)	44(9)	44(3)	26(5)

*：LEE領域にコードされているエフェクター．**：各エフェクターファミリーをコードする遺伝子数(括弧内の数字は偽遺伝子の数)．

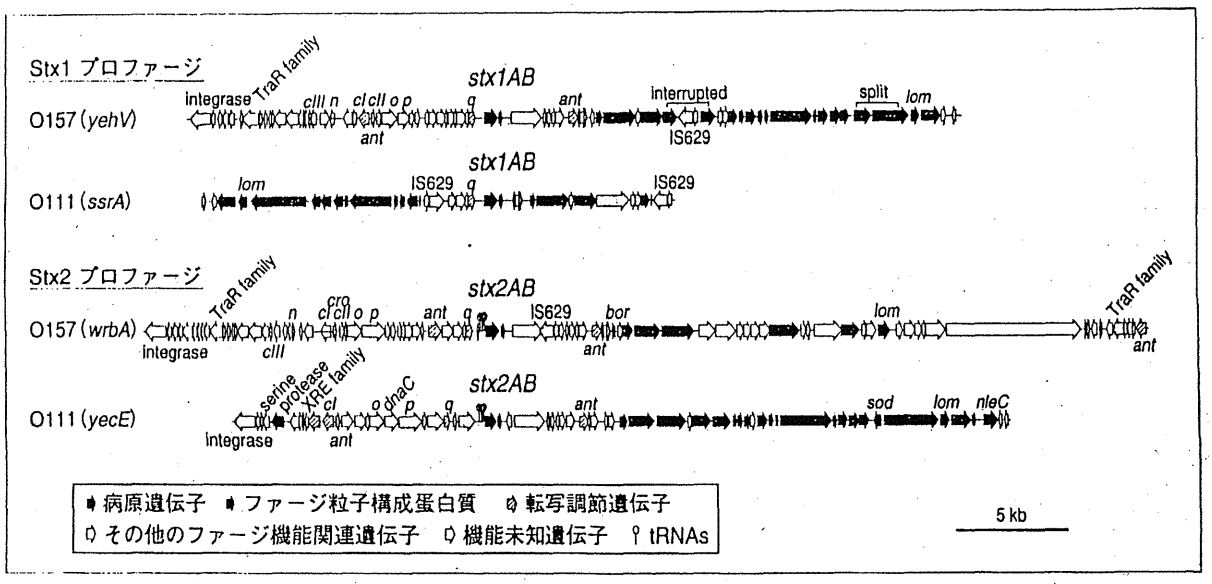

図4　O157とO111のStxファージの比較
いずれのファージもラムダファージの仲間であるが(ラムダ様ファージ)，染色体への挿入部位(括弧内)もファージゲノムの構造もさまざまである．

病原性は，それぞれの病原型に特有な外来性の病原遺伝子群を獲得することによってそれぞれの病原型を示す病原株へと進化したと考えられる．したがって，ここではまずO157やO111などの典型的なEHECが出現した進化過程について解説する．

O157のゲノム解析から明らかになったもっとも重要な点はO157が大量の外来性DNAを獲得していることである．O157には非病原性大腸菌K-12株には存在しない1,500 kbものゲノム配列が存在し，そのほとんどはO157のゲノム上に多数存在するファージやファージ様の遺伝因子，あるいはプラスミドに由来する外来性のDNAである．そこには1,700もの遺伝子がコードされており(当然K-12株には存在しない)，この中に*stx*遺伝子やT3SSの遺伝子群をはじめとする多数の病原遺伝子が存在する．したがって，O157は多数のファージやファージ様の遺伝因子，あるいはプラスミドを介してO157に特有の病原遺伝子セットを獲得し，その病原性を進化させてきたといえる(図2)．

このような外来性病原遺伝子の獲得の中で特に面白いのはT3SSの進化である．すでに述べたように，LEE領域(これもファージ様の外来性遺伝因子の一つ)の獲得によりO157にはT3SSの基本的な要素(分泌装置と7種のエフェクターなど)が備わっている．しかし，LEE領域とは別に多数のファージがエフェクターをコードする遺伝子を運び込んでおり，O157が産生するT3SSエフェクターは40種類にもなる[12]．したがって，O157のT3SSという病原システムは，LEE領域に加えて，多数のファージが次々と感染して多数のエフェクターなどを持ち込むことによって進化した複雑なシステムといえる．

一方，O111, O26, O103にも多数のファージやファージ様の遺伝因子が感染しており，プラスミドも存在する(図3)．O111の場合，ゲノム上に存在する全遺伝子数(蛋白質をコードするもの)は5,732であるが，このうち2,069遺伝子はK-12株には存在しない．そして，これらの外来性遺伝子群のなかにO157のものと非常によく似た病原遺伝子セットが存在する．T3SS関連遺伝子群についても同様で，O111にも類似のエフェクター群が多数のファージによって持ち込まれている(表1)．したがって，図2に示したO157の進化のスキームは，これらO111にも当てはまる[11]．

面白いことに，すべての大腸菌に保存されているゲノム配列に基づいた進化系統解析の結果では，これらのnon-O157 EHECはいずれもO157とは独立に進化してきた大腸菌株である．また，同じ病原遺伝子を運んでいるファージ(たとえばStxをコードするファージ)はO157のものとO111

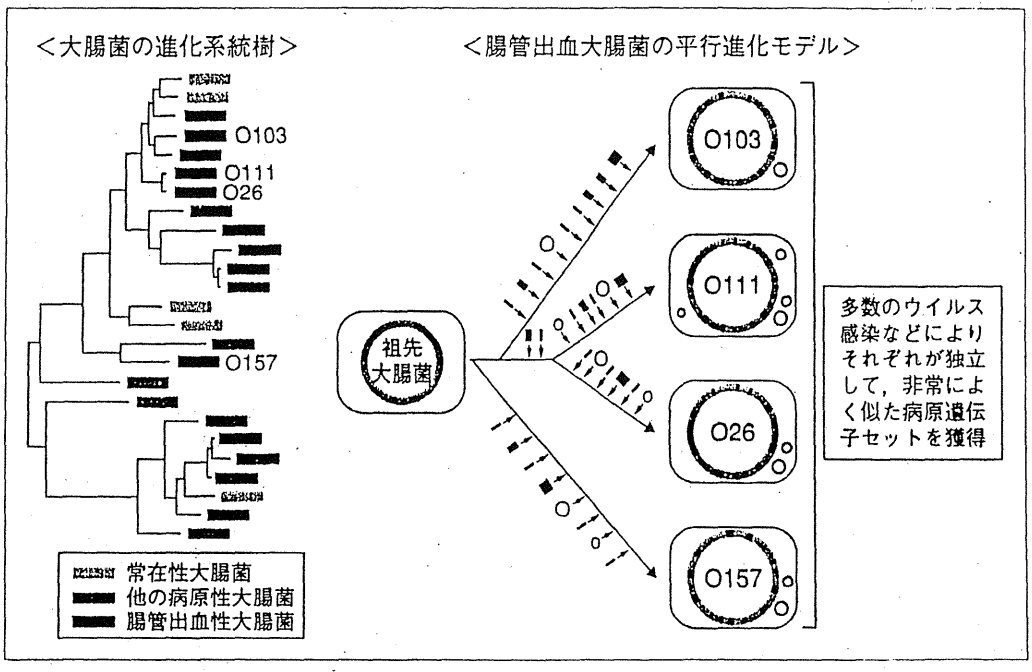

図5　EHECのパラレル進化のメカニズム
左図は各種大腸菌に保存されている900遺伝子の配列を基に作成した系統樹の模式図．O157，O111，O26，O103などのEHECはそれぞれ異なる系統の大腸菌株であることがわかる．

のものとでは同じではない(図4)．同様に，O111が保有する5種類のプラスミドのうちの一つにはO157のプラスミドと同じ病原遺伝子(溶血毒素やプロテアーゼなど)がコードされているが，プラスミド自体の構造は異なる(図3)．したがって，同じファージやプラスミドがO157とO111の間でやり取りされたわけではなく，それぞれが独自にファージやプラスミドなどを獲得することで，結果的に同じような病原遺伝子をセットし，同じような病原性を持った大腸菌として出現したと考えてよい(図5)．なぜこういった一種の収斂進化が生じたのかは不明であり，さまざまな議論があるが，このような進化は「EHECの平行進化(parallel evolution of EHEC)」と呼ばれている[11)13)]．

2．O111の病原性メカニズム

O111もO157と同様にウシなどの腸管(直腸末端部)に定着していると考えられる．O111の場合は仔ウシで腸炎(下痢症)を発症することがあるが(この点はO157と異なる)，ウシはStxに対する感受性がないため，少なくとも成牛はキャリアーとなる．ただし，ウシなどの保有率に関するデータはない．なお，ウシ腸管への定着にはT3SSが関与しているという報告もあるが，詳細なメカニズムは不明である．

一方，ヒトへの感染と発症の過程は，(i)O111に汚染された肉・野菜などの食品や水など経口摂取，(ii)腸管への定着，(iii)腸炎(下痢症)あるいは出血性大腸炎の発症，(iv)HUSや脳症などの合併症の発症に分けて考えることができる．

(i)のステップで重要な点は，EHECが胃酸耐性を有することであり，このため，ごく少量の生菌で発症する(O157のデータでは10～100個の生菌で発症しうる)．このため，汚染食品の流通により大規模な集団感染や広域集団感染(diffuse outbreak)が発生し，家族内での二次感染も生じる．

(ii)のステップでは，まずなんらかの定着因子により初期定着が生じ，続いてT3SSによって上皮細胞内に注入されたTirと細菌細胞のインチミンが結合してattaching and effacing lesionが形成され，上皮細胞への強固な付着が完成する(図1)．初期付着にかかわる因子については完全には明らかとなっていないが，O111のゲノム上にはO157と同様に，10種類以上の線毛や数種類の非線毛性定着因子がコードされており(図2)，これらの因子のいずれか，あるいは組み合わせによって初期付着が生じると考えられる．

(iii)のステップでは，T3SSによって上皮細胞内に注入されるエフェクター群が主役となり，腸炎とそれに伴う下痢症がひき起こされる(図1)．40種類以上にも及ぶエフェクター群については，多くの研究グループによって精力的な研究が進められているが，宿主細胞内での標的や機能や感染過程での発現時期などが完全に明らかになっているものの数は限られている[14]．また，その機能は細胞骨格の改変，タイトジャンクションの傷害，ミトコンドリアの破壊，アポトーシスの阻害，炎症の抑制など多岐にわっており(表1)，このステップを分子レベルで説明できる段階に至っていない．

T3SSによる腸炎はEPECでも生じるが，激しい腹痛と出血を特徴とする出血性大腸炎はEHECに特有の症状である．これにはHUSや脳症などの合併症と同様に，Stxが主要な役割(血管内皮の傷害など)を果たしていると考えられるが，プラスミドにコードされるプロテアーゼや溶血毒素なども関与している可能性もある．

(iv)のステップでは，Stxが決定的な役割を演じる．StxにはStx1(Stxのプロトタイプである志賀赤痢菌*S. dysenteriae*の産生するStxが含まれる)とStx2(Stx2b, 2c, 2eなどのバリアントも存在)の二つのタイプが存在し，いずれもファージにコードされている(図3)．Stxが血中に移行するメカニズムは明らかになっていないが，血中に入ったStxは糖脂質であるglobotriaosylceramide(Gb3)をレセプターとして標的細胞に結合して細胞質内に侵入する．Stxはもっとも強力な細菌毒素の一つであり，28SリボゾームRNA上の特定のadenosine残基を切断(N-glycosidase活性)することによって蛋白合成を阻害し，細胞毒性を発揮する．O111を含むEHECは株によって，Stx1とStx2の両方，あるいはどちらか一方を産生するが，Stx2産生株の方がHUSなどを発症する頻度が高いことが知られており，マウスなどでの実験でもStx1に比べてStx2の方がはるかに高い致死毒性を示す．

StxのレセプターであるGb3は腎臓や中枢神経などで特に多く発現しており，Stxが糸球体内皮を傷害することによりHUSが，また，中枢神経系の血管内皮あるいは神経細胞を傷害することによって脳症がひき起こされる．プロテアーゼや溶血毒素なども副次的な役割を果たしている可能性があるが，よくわかっていない．なお，ウシやブタなどの細胞には，このレセプターが発現していないためStxに対する感受性がない．

Stxに関しては，抗菌薬使用との関係について特に注意すべきである．産生されたStxは菌体内(ペリプラズム)に蓄積されており，βラクタムなどの殺菌的な抗菌薬の投与によって溶菌すると，大量のStxが腸管内に放出される．また，Stxファージは染色体上に組み込まれたプロファージの状態にあり，ニューキノロンのような細菌のDNA複製を阻害する抗菌薬が作用すると，ファージの誘導が起きて大量のファージが産生され，この際に大量のStxの産生と放出が起きる(特にStx2ファージの場合)．したがって，EHEC感染症の場合は(血性の下痢症患者など，EHEC感染症が疑われる場合でも)，抗菌薬の使用についてきわめて慎重でなければならない．ただし，抗菌薬の使用法に関しては米国とヨーロッパで異なり，わが国でも一定の方針は示されていないのが現状である．

今後の展望

腸管出血性大腸菌O111自体を対象とした研究が少ないのが現状であるが，国内でも国外でも，O157以外のenterohemorrhagic *E. coli*(EHEC)の重要性にも注目が集まってきており，今後はO111を対象とする研究も活発化すると予想される．全ゲノム情報が明らかになったことも，この流れを後押しすると考えられる(O111での病原性解析など)．特に重要と考えられるのは，リザーバーとなっているウシなどでの保有率を明らかにすること，および多様なO111株を解析することで菌株間での性状やゲノムの違いを明らかにすることの2点であろう．株間の多様性に関する解析はO157では活発に進んでおり[15)~18)]，われわれのグループでは，その成果を応用したO157の迅速菌株識別法なども開発している[19)]．また，米国のグループからは，HUSの合併など重症化感染をひき起こすリスクが高い特定のO157系統の存在が報告されている[20)21)]．この点に関連して興味深いのは，2011年に富山を中心に発生したO111

集団感染事例では，過去に国内で発生した他のO111集団感染よりも重症化率が高いと報告されていることであり，他のO111株との比較(たとえばゲノム比較)などを積極的に進める必要があると思われる．また，他のnon-O157 EHECのいずれもが重大な集団感染をひき起こす可能性を秘めており，non-O157 EHEC全般に対する研究を積極的に推進していくことが重要であろう．

文　献

1) Nataro JP, Kaper JB. Diarrheagenic *Escherichia coli*. C Microbiol Rev 1998 ; 11 : 142-201.
2) Kaper JB, Nataro JP, Mobley HL. Pathogenic *Escherichia coli*. Nat Rev Microbiol 2004 ; 2 : 123-40.
3) Croxen MA, Finlay BB. Molecular mechanisms of *Escherichia coli* pathogenicity. Nat Rev Microbiol 2010 ; 8 : 26-38.
4) Karmali MA, Mascarenhas M, Shen S, et al. Association of genomic O island 122 of *Escherichia coli* EDL 933 with verocytotoxin-producing *Escherichia coli* seropathotypes that are linked to epidemic and/or serious disease. J Clin Microbiol 2003 ; 41 : 4930-40.
5) Mellmann A, Bielaszewska M, Köck R, et al. Analysis of collection of hemolytic uremic syndrome-associated enterohemorrhagic *Escherichia coli*. Emerg Infect Dis 2008 ; 14 : 1287-90.
6) Frank C, Werber D, Cramer JP, et al. Epidemic profile of Shiga-toxin-producing *Escherichia coli* O104 : H4 outbreak in Germany. N Engl J Med 2011 ; 365 : 1771-80.
7) Rohde H, Qin J, Cui Y, et al. Open-source genomic analysis of Shiga-toxin-producing *E. coli* O104 : H4. N Engl J Med 2011 ; 365 : 718-24.
8) Rasko DA, Webster DR, Sahl JW, et al. Origins of the *E. coli* strain causing an outbreak of hemolytic-uremic syndrome in Germany. N Engl J Med 2011 ; 365 : 709-17.
9) Perna NT, Plunkett G 3rd, Burland V, et al. Genome sequence of enterohaemorrhagic *Escherichia coli* O157 : H7. Nature 2001 ; 409 : 529-33.
10) Hayashi T, Makino K, Ohnishi M, et al. Complete genome sequence of enterohemorrhagic *Escherichia coli* O157 : H7 and genomic comparison with a laboratory strain K-12. DNA Res 2001 ; 8 : 11-22.
11) Ogura Y, Ooka T, Iguchi A, et al. Comparative genomics reveal the mechanism of the parallel evolution of O157 and non-O157 enterohemorrhagic *Escherichia coli*. Proc Natl Acad Sci USA 2009 ; 106 : 17939-44.
12) Tobe T, Beatson SA, Taniguchi H, et al. An extensive repertoire of type III secretion effectors in *Escherichia coli* O157 and the role of lambdoid phages in their dissemination. Proc Natl Acad Sci USA 2006 ; 103 : 14941-6.
13) Reid SD, Herbelin CJ, Bumbaugh AC, et al. Parallel evolution of virulence in pathogenic *Escherichia coli*. Nature 2000 ; 406 : 64-7.
14) Wong AR, Pearson JS, Bright MD, et al. Enteropathogenic and enterohaemorrhagic *Escherichia coli* : even more subversive elements. Mol Microbiol 2011 ; 80 : 1420-38.
15) Ohnishi M, Terajima J, Kurokawa K, et al. Genomic diversity of enterohemorrhagic *Escherichia coli* O157 revealed by whole genome PCR scanning. Proc Natl Acad Sci USA 2002 ; 99 : 17043-8.
16) Zhang W, Qi W, Albert TJ, et al. Probing genomic diversity and evolution of *Escherichia coli* O157 by single nucleotide polymorphisms. Genome Res 2006 ; 16 : 757-67.
17) Ooka T, Ogura Y, Asadulghani M, et al. Inference of the impact of insertion sequence (IS) elements on bacterial genome diversification through analysis of small-size structural polymorphisms in *Escherichia coli* O157 genomes. Genome Res 2009 ; 19 : 1809-16.
18) Leopold SR, Magrini V, Holt NJ, et al. A precise reconstruction of the emergence and constrained radiations of *Escherichia coli* O157 portrayed by backbone concatenomic analysis. Proc Natl Acad Sci USA 2009 ; 106 : 8713-8.
19) Ooka T, Terajima J, Kusumoto M, et al. Development of a multiplex PCR-based rapid typing method for enterohemorrhagic *Escherichia coli* O157 strains. J Clin Microbiol 2009 ; 47 : 2888-94.
20) Manning SD, Motiwala AS, Springman AC, et al. Variation in virulence among clades of *Escherichia coli* O157 : H7 associated with disease outbreaks. Proc Natl Acad Sci USA 2008 ; 105 : 4868-73.
21) Laing CR, Buchanan C, Taboada EN, et al. In silico genomic analyses reveal three distinct lineages of *Escherichia coli* O157 : H7, one of which is associated with hyper-virulence. BMC Genomics 2009 ; 10 : 287.

Infection and Immunity

Subtilase Cytotoxin Enhances Escherichia coli Survival in Macrophages by Suppression of Nitric Oxide Production through the Inhibition of NF- κB Activation

Hiroyasu Tsutsuki, Kinnosuke Yahiro, Kotaro Suzuki, Akira Suto, Kohei Ogura, Sayaka Nagasawa, Hideshi Ihara, Takeshi Shimizu, Hiroshi Nakajima, Joel Moss and Masatoshi Noda

Infect. Immun. **2012, 80(11):3939. DOI: 10.1128/IAI.00581-12. Published Ahead of Print 4 September 2012.**

IAI
Journals.ASM.org

Subtilase Cytotoxin Enhances *Escherichia coli* Survival in Macrophages by Suppression of Nitric Oxide Production through the Inhibition of NF-κB Activation

Hiroyasu Tsutsuki,[a] Kinnosuke Yahiro,[a] Kotaro Suzuki,[b] Akira Suto,[b] Kohei Ogura,[a] Sayaka Nagasawa,[c] Hideshi Ihara,[d] Takeshi Shimizu,[a] Hiroshi Nakajima,[b] Joel Moss,[e] and Masatoshi Noda[a]

Departments of Molecular Infectiology,[a] Molecular Genetics,[b] and Legal Medicine,[c] Graduate School of Medicine, Chiba University, Chiba, Japan; Department of Biological Science, Graduate School of Science, Osaka Prefecture University, Osaka, Japan[d]; and Cardiovascular and Pulmonary Branch, National Heart, Lung, and Blood Institute, National Institutes of Health, Bethesda, Maryland, USA[e]

Subtilase cytotoxin (SubAB), which is produced by certain strains of Shiga-toxigenic *Escherichia coli* (STEC), cleaves an endoplasmic reticulum (ER) chaperone, BiP/Grp78, leading to induction of ER stress and caspase-dependent apoptosis. SubAB alters the innate immune response. SubAB pretreatment of macrophages inhibited lipopolysaccharide (LPS)-induced production of both monocyte chemoattractant protein 1 (MCP-1) and tumor necrosis factor α (TNF-α). We investigated here the mechanism by which SubAB inhibits nitric oxide (NO) production by mouse macrophages. SubAB suppressed LPS-induced NO production through inhibition of inducible NO synthase (iNOS) mRNA and protein expression. Further, SubAB inhibited LPS-induced IκB-α phosphorylation and nuclear localization of the nuclear factor-κB (NF-κB) p65/p50 heterodimer. Reporter gene and chromatin immunoprecipitation (ChIP) assays revealed that SubAB reduced LPS-induced NF-κB p65/p50 heterodimer binding to an NF-κB binding site on the iNOS promoter. In contrast to the native toxin, a catalytically inactivated SubAB mutant slightly enhanced LPS-induced iNOS expression and binding of NF-κB subunits to the iNOS promoter. The SubAB effect on LPS-induced iNOS expression was significantly reduced in macrophages from NF-κB1 (p50)-deficient mice, which lacked a DNA-binding subunit of the p65/p50 heterodimer, suggesting that p50 was involved in SubAB-mediated inhibition of iNOS expression. Treatment of macrophages with an NOS inhibitor or expression of SubAB by *E. coli* increased *E. coli* survival in macrophages, suggesting that NO generated by macrophages resulted in efficient killing of the bacteria and SubAB contributed to *E. coli* survival in macrophages. Thus, we hypothesize that SubAB might represent a novel bacterial strategy to circumvent host defense during STEC infection.

Shiga-toxigenic *Escherichia coli* (STEC) produces Shiga toxin 1 (Stx1) and Stx2, which are cytotoxic for colon cells, resulting in hemorrhagic colitis. Shiga toxins are significant virulence factors in STEC infection and may be responsible for life-threatening complications, such as hemolytic-uremic syndrome (HUS) (27, 43). However, it is not clear whether Shiga toxins are the only factors responsible for the morbidity and mortality associated with STEC-associated disease.

A new member of the AB_5 toxin family, named subtilase cytotoxin (SubAB), was identified in *E. coli* O113:H21 strain 98NK2, which produces Stx2 and was responsible for an outbreak of HUS (42). SubAB binds to receptors on the cell membrane (59, 60) and thereby enters the cell, resulting in a site-specific cleavage of endoplasmic reticulum (ER) chaperone protein BiP/Grp78. Previous studies have shown that BiP/Grp78 cleavage by SubAB initiates an ER stress-induced unfolded protein response (UPR) (41, 54), resulting in transient inhibition of protein synthesis (34), G_0/G_1 cell cycle arrest (33, 34), downregulation of gap junction expression (24), and caspase-dependent apoptosis via mitochondrial membrane damage (32, 58). These actions of SubAB are responsible for cell death and may be involved in STEC-induced disease. Intriguingly, in addition to these activities, a series of recent studies showed that SubAB pretreatment of various cell lines inhibited lipopolysaccharide (LPS)- and tumor necrosis factor alpha (TNF-α)-induced NF-κB activation (17, 37). SubAB inhibition of TNF-α-induced NF-κB activation in rat renal tubular epithelial cells resulted from induction of CCAAT/enhancer-binding protein beta (C/EBPβ) and a mammalian target of rapamycin (mTOR)-dependent Akt phosphorylation pathways (37). However, an early event following SubAB-induced ER stress involved activation of NF-κB through an Akt-dependent pathway (61).

Nitric oxide (NO) is a short-lived free radical and an internal messenger that mediates a variety of functions, including vascular homeostasis, neurotransmission, and host defense (30). NO is synthesized from L-arginine by NO synthases (NOS) (2, 30). In mammals, three different isoforms of NOS exist (i.e., neuronal [nNOS], inducible [iNOS], and endothelial [eNOS]). nNOS and eNOS are primarily expressed in neurons and endothelial cells, respectively. In contrast, iNOS is a primary regulator of NO production in the innate immune system whose expression can be induced by LPS, gamma interferon (IFN-γ), interleukin-1β (IL-1β), IL-6, and TNF-α (2). iNOS gene expression is regulated through transcriptional control, particularly by NF-κB activation

Received 29 May 2012 Returned for modification 13 July 2012
Accepted 25 August 2012
Published ahead of print 4 September 2012
Editor: S. M. Payne
Address correspondence to Kinnosuke Yahiro, yahirok@faculty.chiba-u.jp.

doi:10.1128/IAI.00581-12

(29, 56, 57). Five mammalian NF-κB subunits, p65 (RelA), RelB, c-Rel, NF-κB1 (p50 and its precursor, p105), and NF-κB2 (p52 and its precursor, p100), form homo- or heterodimers to produce gene regulatory complexes with different properties (10, 46). In LPS-induced iNOS expression, the involvement of the NF-κB p65/p50 heterodimer is well documented (10). p65/p50 heterodimer is held in an inactive state in the cytoplasm by IκB, which is phosphorylated by the IκB kinase (IKK) complex (9), leading to IκB degradation and NF-κB activation (26). In mouse, the iNOS gene promoter contains two NF-κB binding sites, one upstream (GGGATTTTCC; nucleotides −971 to −962, designated the NF-κBu site) and one downstream (GGGACTCTCC; nucleotides −85 to −76, designated the NF-κBd site), both of which need to be occupied to obtain full induction of iNOS by LPS (56).

Phagocytic cells such as macrophages or neutrophils are important components of the innate immune response. Two major antimicrobial systems of phagocytic cells are the NADPH phagocyte oxidase (also known as phox) and iNOS pathways, which are responsible for the generation of superoxide (O_2^-) and NO, respectively (11). The NO produced by iNOS contributes to the bactericidal activities of macrophages. NO reacts with simultaneously generated reactive oxygen species (ROS), resulting in formation of reactive nitrogen species (RNS), such as peroxynitrite ($ONOO^-$) and nitrogen dioxide (NO_2). NO, RNS, and ROS have antimicrobial activities (39). NO potentiates hydrogen peroxide (H_2O_2)-induced killing of *E. coli* in part through the generation of $ONOO^-$ (3, 40). Nitrite exerts antimicrobial effects through generation of NO, which is toxic to STEC (35). Furthermore, NO suppresses Stx2 production by STEC through inhibition of stx_2 mRNA expression (51). These findings suggest that NO and NO-derived RNS protect the host from STEC-induced disease.

In this study, we demonstrate in mouse macrophages that SubAB inhibited LPS-stimulated NO production through inhibition of NF-κB nuclear translocation and iNOS expression. Moreover, we show that NF-κB p50 is involved in inhibition of LPS-induced iNOS expression by SubAB. In addition, we report that SubAB enhanced *E. coli* survival in macrophages. This study provides the first evidence for direct inhibition by SubAB of LPS-induced, NF-κB activation-mediated NO production and for a novel bacterial strategy to survive in macrophages.

MATERIALS AND METHODS

Reagents. LPS (from *Escherichia coli* O111:B4), penicillin-streptomycin, polymyxin B, and anti-α-tubulin monoclonal antibody were purchased from Sigma-Aldrich (St. Louis, MO). Dulbecco's modified Eagle's medium (DMEM) and fetal bovine serum (FBS) were obtained from Gibco BRL (Grand Island, NY). All primers were synthesized chemically by Invitrogen (Carlsbad, CA). Anti-NF-κB p65 polyclonal antibodies (C-20, sc-372), anti-NF-κB p50 polyclonal antibodies (H-119, sc-7178), and anti-NF-κB p50 monoclonal antibodies (E-10, sc-8414) were purchased from Santa Cruz Biotechnology; anti-NF-κB p50 polyclonal antibodies and mouse recombinant M-CSF were from eBioscience; anti-nucleoporin p62 and anti-BiP/Grp78 monoclonal antibodies were from BD Bioscience; anti-phospho-IκB-α monoclonal antibody (9246) and recombinant TNF-α were from Cell Signaling; and anti-GAPDH polyclonal antibodies were from GeneTex. L-NAME was from DOJINDO (Kumamoto, Japan). Other reagents were purchased from Wako Pure Chemical Industries (Osaka, Japan). iNOS-specific monoclonal antibody i2G4 was prepared as described previously (38).

Animals. NF-κB1$^{-/-}$ mice (46) were purchased from the Jackson Laboratories (Bar Harbor, ME) and C57BL/6J wild-type mice from SLC (Hamamatsu, Japan). Animal experiments were approved by Chiba University Institutional Animal Care and Use Committee, Chiba, Japan.

Preparation of SubAB. Recombinant His-tagged SubAB and a catalytically inactive SubAB mutant, $SubA_{S272A}B$ (mSubAB), were purified as reported previously (34). Heat-inactivated SubAB (Hi-SubAB) and heat-inactivated mSubAB (Hi-mSubAB) were prepared as described previously (59).

Cell culture and treatment. RAW 264.7 cells, a murine macrophage cell line, were obtained from Riken Cell Bank (Tsukuba, Japan) and maintained in Dulbecco's modified Eagle's medium (DMEM) containing 10% heat-inactivated fetal bovine serum (FBS), 100 U/ml penicillin, and 0.1 mg/ml streptomycin (DMEM-10% FBS) at 37°C under 5% CO_2. The preparation of bone marrow macrophages (BMMs) from NF-κB1$^{-/-}$ mice was based on the procedure of Guilbert and Stanley (16). Briefly, bone marrow cells were collected from the femurs and tibiae of mice and cultured in DMEM-10% FBS, supplemented with 20 ng/ml M-CSF, for 4 to 6 days before use in experiments. RAW 264.7 cells and BMMs were stimulated with LPS (0.01 to 10 μg/ml) or recombinant TNF-α (10 ng/ml) in the presence or absence of SubAB (0.005 to 1 μg/ml) or mSubAB (0.5 μg/ml) in DMEM containing 1% heat-inactivated FBS, 100 U/ml penicillin, and 0.1 mg/ml streptomycin (DMEM-1% FBS) as described in the figure legends.

Analysis of nitrite accumulation. NO release from macrophage cells was determined by assaying nitrite levels, a relatively stable NO metabolite. The accumulation of nitrite in culture supernatants was quantified by Griess reaction, as described previously (47). Briefly, cells were stimulated as described in the figure legends and 50-μl aliquots of the culture supernatants were dispensed in triplicate into 96-well plates and mixed with 25 μl of Griess reagent A (1% sulfanilamide in 5% H_3PO_4). After 5 min of incubation, 25 μl of Griess reagent B [0.1% *N*-(1-naphthyl)-ethylenediamine] was added, followed by incubation for 10 min at room temperature. The absorbance of samples at 540 nm was compared with that of sodium nitrite standard on a microplate reader (Bio-Rad).

Cell viability assay. RAW 264.7 cells were incubated with 0.5 μg/ml of SubAB, mSubAB, Hi-SubAB, and Hi-mSubAB for 24 or 48 h, and cell viability was evaluated by cell counting kit 8 (DOJINDO), according to the manufacturer's protocol.

Preparation of total cell lysate and cytoplasmic and nuclear protein extracts. To prepare total cell lysate, cells were treated with LPS in the presence or absence of SubAB or mSubAB, washed with phosphate-buffered saline (PBS), and lysed with SDS sample buffer (62.5 mM Tris-HCl [pH 6.8], 1% SDS, 10% glycerol, 2.5% mercaptoethanol, and 0.001% bromophenol blue). Cytoplasmic and nuclear protein extracts were prepared as described previously (45). Briefly, cells were washed with ice-cold PBS and then incubated with hypotonic lysis buffer (10 mM HEPES [pH 8.0], 2 mM $MgCl_2$, 1 mM $CaCl_2$, and 10% glycerol) containing protease inhibitor (PI) cocktail (Complete ULTRA, mini, EDTA free) (Roche Diagnostics) on ice for 10 min. Nonidet P-40 was added to a final concentration of 0.6%, and the resulting preparation was vortexed for 10 s and then centrifuged at 10,000 × *g* for 30 s. Nuclear pellets were washed with hypotonic lysis buffer, and nuclear proteins were extracted by incubation of the nuclei with nuclear extract buffer (20 mM HEPES [pH 8.0], 0.42 M NaCl, 0.5 mM dithiothreitol [DTT], and 10% glycerol) containing PI cocktail for 15 min at 4°C, and cell debris was removed by centrifugation at 15,000 × *g* for 15 min at 4°C. The Bradford method (protein assay; Bio-Rad) was used to measure protein concentration in the extract, which was then stored in aliquots at −80°C.

Immunoprecipitation. Coimmunoprecipitation of NF-κB p50 and p65 was carried out as described previously (60). Briefly, cytoplasmic proteins were incubated with anti-NF-κB p50 antibody (Santa Cruz Biotechnology) at 4°C overnight. Immunoprecipitates were collected by incubation with protein G-Sepharose (Invitrogen) for 1 h, followed by centrifugation for 1 min at 4°C. Immunocomplexes were washed with hypotonic lysis buffer three times, and proteins were dissolved in sodium dodecyl sulfate (SDS) sample buffer, subjected to SDS-polyacrylamide gel

electrophoresis (PAGE) in 7.5% gels, transferred to polyvinylidene difluoride (PVDF) membranes, and then analyzed by Western blotting using anti-NF-κB p65 antibodies (Santa Cruz Biotechnology).

Immunostaining. RAW 264.7 cells were seeded in 12-well plates containing coverslips and incubated at 37°C overnight. After treatment as described in the figure legends, the cells were fixed with 4% formaldehyde in PBS at room temperature for 15 min and then washed three times with PBS. Cells permeabilized with methanol for 10 min at −20°C were treated with PBS containing 5% goat serum and 0.05% Triton X-100 for 1 h. Cells were incubated with anti-NF-κB p65 polyclonal antibodies or anti-NF-κB p50 monoclonal antibody overnight at 4°C and washed three times with PBS, followed by incubation at room temperature for 1 h with Cy3-conjugated anti-rabbit IgG or Alexa 488-conjugated anti-mouse IgG. Cells on the coverslips were then washed three times with PBS, once with water, dried, and mounted on glass slides using ProLong Gold antifade reagent with DAPI (4′,6-diamidino-2-phenylindole) (Invitrogen). Stained cells were visualized using confocal microscopy (Olympus).

Immunoblotting analysis. Total cell lysate and cytoplasmic and nuclear extracts lysed in SDS sample buffer were heated at 100°C for 5 min before proteins were analyzed by SDS-PAGE. After electrophoresis at room temperature, separated proteins were transferred to PVDF membranes at 100 V for 1 h. Membranes were blocked with 5% nonfat milk in TBS-T (20 mM Tris-HCl [pH 7.6], 137 mM NaCl, 0.1% Tween 20) for 30 min and then incubated with primary antibodies for 1 h at room temperature or overnight at 4°C. After being washed five times for 5 min with TBS-T, membranes were incubated with horseradish peroxidase-labeled secondary antibodies. Bands were visualized using Las 1000 (Fuji film).

Quantitative reverse-transcription PCR (qRT-PCR). Total RNA was prepared from RAW 264.7 cells or BMMs using the PureLink RNA mini-kit (Invitrogen), according to the manufacturer's protocol. Total RNA was measured, and 1 to 5 μg were reverse transcribed using Ready-To-Go You-Prime first-strand beads (GE Healthcare) with oligo(dT)$_{12-18}$ primer (Invitrogen). cDNA content was measured by real-time PCR with SYBR green reagent using an ABI PRISM 7300 sequence detection system (Applied Biosystems, Foster City, CA). Specific primers used for real-time PCR were as follows: mouse iNOS forward, 5′-GTTCTCAGCCCAACAA TACAAGA-3′, and reverse, 5′-GTGGACGGGTCGATGTCAC-3′. Primers for GAPDH cDNA amplification were as described previously (13).

Plasmids, transient transfection, and reporter gene assay. The mouse iNOS promoter-luciferase reporter plasmid (pGL2-iNOS) was generously provided by Charles J. Lowenstein (Johns Hopkins University) via Addgene Inc. (Addgene plasmid 19296). Deletion constructs were created by modified methods as reported (29). All constructs were then sequenced to characterize them definitively. Endotoxin-free plasmid DNA was purified using Qiagen plasmid plus midikit (Qiagen), according to the manufacturer's protocol. RAW 264.7 cells (1×10^4 or 2.5×10^4 cells) transfected with a luciferase reporter plasmid were cultured in 24-well plates in DMEM-1% FBS. Reporter constructs (pGL2-iNOS; 0.5 μg or HIV-NF-κB luciferase reporter construct [9]; 1.5 μg) were mixed with 20 ng of phRL-TK (Promega) in 50 μl of Opti-MEM I reduced serum medium (GIBCO/Invitrogen). The solution was mixed with 1 μl of FuGENE 6 (Roche Diagnostics) and incubated at room temperature for 30 min; the two vectors in 50-μl solutions were cotransfected into RAW 264.7 cells after the medium was replaced with 300 μl of fresh DMEM-10% FBS. Subsequently, the cells were incubated at 37°C for 24 or 72 h. After transfection with plasmid, the medium was replaced with 300 μl of fresh DMEM-1% FBS and cells were stimulated with LPS (10 μg/ml) in the presence or absence of SubAB or mSubAB. After incubation for 4, 8, or 24 h, cells were washed with cold PBS and lysed by adding 100 μl of passive lysis buffer (Promega). Aliquots of 20 μl of cell lysate were used to assay for luciferase activity with the dual-luciferase reporter assay kit (Promega), according to the manufacturer's guidelines.

ChIP-qPCR assays. Chromatin immunoprecipitation (ChIP)-qPCR assays were performed to examine the binding of NF-κB p65 and p50 subunits to iNOS promoter, as reported previously (22). Briefly, cells were fixed with 1% formaldehyde for 10 min at 37°C, collected by scraping, and lysed in SDS buffer (50 mM Tris-HCl [pH 8.1], 10 mM EDTA, 1% SDS) containing protease inhibitor cocktail (Roche Diagnostics). Lysates were sonicated to fragment the chromatin by using Bioruptor (Cosmo Bio Co., Tokyo, Japan) and then diluted with ChIP dilution buffer (20 mM Tris-HCl [pH 8.1], 1 mM EDTA, 150 mM NaCl, and 0.3% Triton X-100). Immunoprecipitation analysis was carried out using control rabbit IgG and anti-NF-κB p65 or anti-NF-κB p50 antibodies. Cross-links were reversed at 65°C for 6 h, and proteins were digested with proteinase K (0.4 mg/ml) for 1 h at 55°C. Immunoprecipitated DNA was recovered by the QIAQiuck PCR purification kit (Qiagen). DNA fragments were amplified by PCR with specific primers as follows: 5′-CACACAGACTAGGAGTGT CCATCAT-3′ and 5′-CATAACTGTTCCCAAAGGGAGAGT-3′. DNA content was measured by real-time PCR with SYBR green reagent using an ABI PRISM 7300 sequence detection system (Applied Biosystems, Foster City, CA). Results are expressed as the percent input for each ChIP fraction.

Macrophage infection. Transformants of *E. coli* strain BL21(DE3) (Invitrogen) carrying the SubAB and mSubAB genes on pET23b (BL21/pET-SubAB and BL21/pET-mSubAB, respectively) were generated as reported previously (34). For macrophage infection, RAW 264.7 cells were cultured in antibiotic-free DMEM containing 10% heat-inactivated FBS and infected as described previously (47). Briefly, cells were seeded at 1×10^6 cells per well in 24-well tissue culture dishes for 24 h and then infected with BL21/pET23b, BL21/pET-SubAB, or BL21/pET-mSubAB at a multiplicity of infection (MOI) of 10. The plate was centrifuged for 5 min at 1,000 × *g* to synchronize the infection and incubated for 20 min, and then the cells were washed and fresh medium containing 100 μg/ml of gentamicin was added to kill extracellular bacteria. After 2 h, the medium was discarded, the cells were washed, and the medium was changed to include 20 μg/ml of gentamicin with or without L-NAME (10 mM), SubAB, or mSubAB. The infected monolayers were lysed on the tissue culture dishes by the addition of 0.1% sodium deoxycholate in phosphate-buffered saline. The number of surviving bacteria was determined by bacterial plate counts (CFU).

Statistical analysis. Student's *t* test was used to determine significant difference when only two treatment groups were being compared. Analysis of variance (ANOVA) with the Student-Newman-Keuls test was used to analyze significant differences among multiple groups.

RESULTS

SubAB inhibits LPS-induced NO production by RAW 264.7 cells. To investigate the effect of SubAB on LPS-induced NO production in RAW 264.7 cells, cells were incubated with LPS for 24 h in the presence or absence of SubAB, a catalytically inactive SubAB mutant (mSubAB), heat-inactivated SubAB, or heat-inactivated mSubAB, and then supernatants were collected for the measurement of nitrite, a relatively stable metabolite of NO (Fig. 1A). When RAW 264.7 cells were incubated with LPS, a significant amount of NO production was observed. LPS-induced NO production was markedly decreased in SubAB-treated RAW 264.7 cells. mSubAB treatment did not inhibit LPS-induced NO production; rather, it slightly increased NO production. Heat-inactivated SubAB or heat-inactivated mSubAB did not affect LPS-induced NO production by RAW 264.7 cells. In addition, LPS-induced NO production was completely reduced in the presence of an iNOS-specific inhibitor 1400W dihydrochloride, indicating that iNOS is essential for LPS-induced NO production by RAW 264.7 cells. These results suggest that SubAB-induced ER stress inhibits LPS-induced NO production by RAW 264.7 cells, and mSubAB binding to RAW 264.7 cells slightly enhances LPS-induced NO production. In addition, SubAB treatment suppressed LPS-induced NO production in a dose-dependent man-

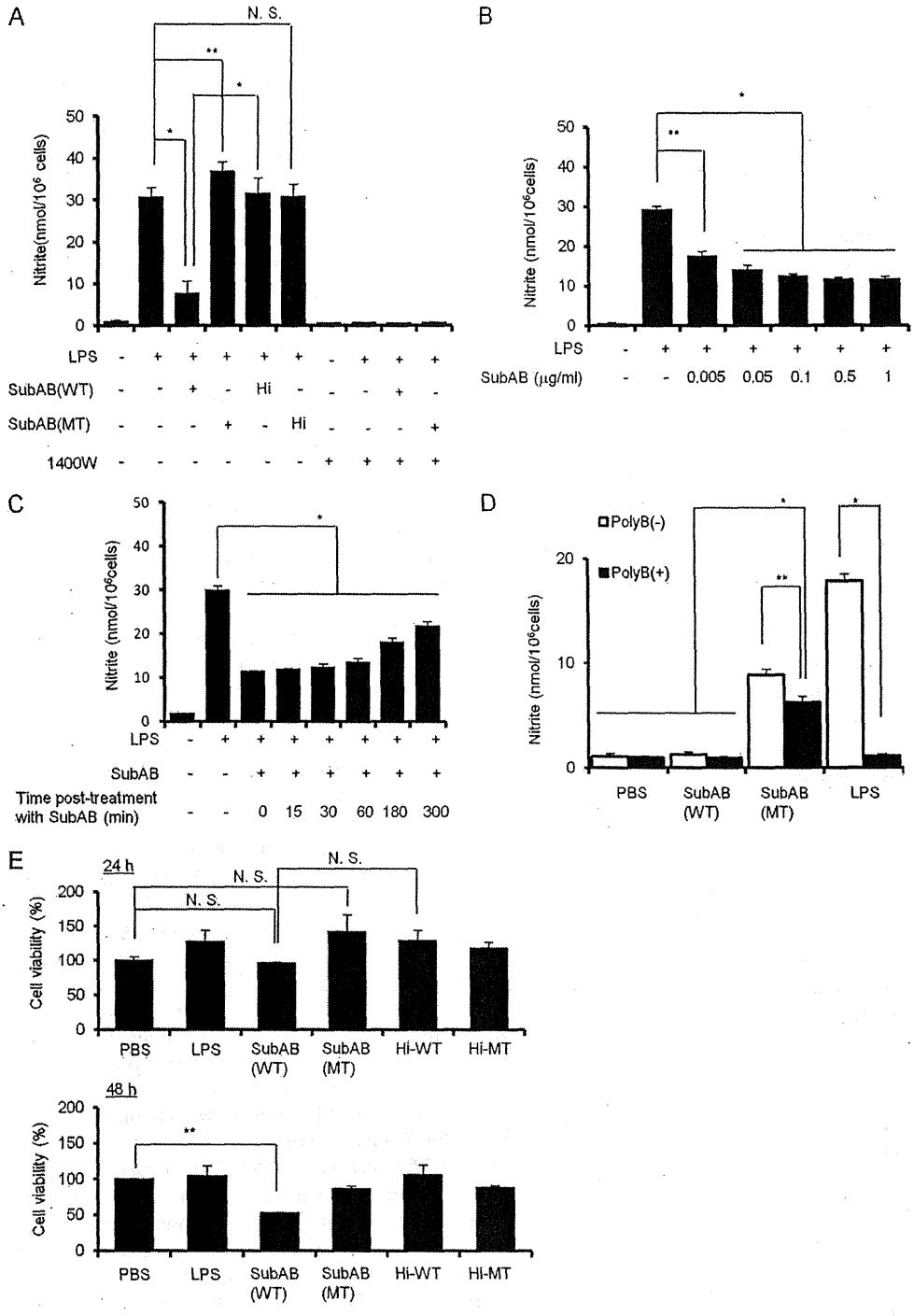

FIG 1 SubAB inhibits LPS-induced nitrite production by RAW 264.7 cells. (A) RAW 264.7 cells (1×10^5 cells/well) in a 96-well dish were grown in DMEM-1% FBS for 24 h. Cells were treated with LPS (10 μg/ml) in the presence or absence of SubAB (0.5 μg/ml), its catalytically inactive mutant, mSubAB (MT), heat-inactivated SubAB (Hi-WT), heat-inactivated mSubAB (Hi-MT) (0.5 μg/ml), or 1400W dihydrochloride for 24 h. The accumulation of nitrite in culture supernatants was quantified by Griess assay, as described in Materials and Methods. (B) RAW 264.7 cells (1×10^5 cells/well) in a 96-well dish were grown in DMEM-1% FBS for 24 h. Cells were treated with LPS (10 μg/ml) in the presence or absence of the indicated concentrations of SubAB (WT) for 24 h. The accumulation of nitrite in culture supernatants was quantified by Griess assay as described above. (C) RAW 264.7 cells (1×10^5 cells/well) in a 96-well dish were grown in DMEM-1% FBS for 24 h. Cells were treated with LPS (10 μg/ml) and then posttreated with SubAB (0.5 μg/ml) after LPS stimulation for 0, 15, 30, 60, 180, and 300 min. After a total incubation time of 24 h, nitrite was quantified by Griess assay as described above. (D) RAW 264.7 cells (1×10^5 cells/well) in a 96-well dish were grown in DMEM-1% FBS for 24 h. Cells were treated with LPS (10 ng/ml), SubAB (WT), or mSubAB (MT) at 0.5 μg/ml for 24 h in DMEM-1% FBS in the presence or absence of polymyxin B (10 μg/ml). The accumulation of nitrite in culture supernatants was quantified as described above. (E) RAW 264.7 cells (1×10^5 cells/well) in a 96-well dish were grown in DMEM-1% FBS for 24 h. Cells were treated with SubAB (WT), mSubAB (MT), heat-inactivated SubAB (Hi-WT), or heat-inactivated mSubAB (Hi-MT) (0.5 μg/ml) for 24 or 48 h. Cell viability was evaluated by cell counting kit 8 (DOJINDO) according to the instruction manual. Data for all these experiments are means ± standard deviations (SD) of values from three independent assays in triplicate experiments. Statistical significance: *, $P < 0.01$; **, $P < 0.05$; N.S., not significant.

ner in RAW 264.7 cells, with 0.5 μg/ml of SubAB inhibiting LPS-induced NO production by RAW 264.7 cells (Fig. 1B). Posttreatment with SubAB after LPS treatment for 0 to 180 min significantly suppressed LPS-induced NO production by RAW 264.7 cells, suggesting that SubAB effectively inhibits NO production (Fig. 1C). The effect of SubAB appeared to be diminished with time. To examine the effect of mSubAB binding on NO production in RAW 264.7 cells, cells were treated with PBS control, LPS (10 ng/ml), SubAB, or mSubAB in the presence or absence of polymyxin B, which inactivates LPS (36, 62). In the absence of polymyxin B, both LPS and mSubAB, but not SubAB, induced NO production. In the presence of polymyxin B, LPS-induced NO production was completely inhibited, but mSubAB-induced NO production was only partially reduced (Fig. 1D). These results suggest that mSubAB binding to cells may promote NO production. mSubAB is known to bind surface receptors, even though it is catalytically inactive. A recent study reported that SubAB inhibits TNF-α-induced NF-κB activation in rat renal tubular epithelial cells (37). To examine the effect of SubAB on TNF-α-induced NO production by RAW 264.7 cells, cells were treated with recombinant mouse or human TNF-α in the presence or absence of SubAB. However, both recombinant mouse and human TNF-α did not induce NO production by RAW 264.7 (data not shown). Next, we tested the effect of SubAB on RAW 264.7 cell viability. At 0.5 μg/ml, SubAB did not affect cell viability at 24 h, but cell death was detected after 48 h (Fig. 1E). Heat-inactivated SubAB or mSubAB or heat-inactivated mSubAB did not affect cell viability. Therefore, we used 0.5 μg/ml SubAB in our experiments.

SubAB inhibits LPS-induced iNOS expression in RAW 264.7 cells. To investigate the mechanism of the inhibitory effects of SubAB on LPS-induced NO production in RAW 264.7 cells, LPS-induced iNOS expression in the presence and absence of SubAB was analyzed by immunoblotting. LPS induced iNOS protein expression in a dose-dependent manner; it was dramatically blocked by SubAB (Fig. 2A). LPS also induced iNOS expression in RAW 264.7 cells in a time-dependent manner, which was attenuated in the presence of SubAB but not mSubAB (Fig. 2B). In addition, densitometric analysis also showed that SubAB suppressed LPS-induced iNOS expression. To test whether the inhibitory effect involved ER stress, we investigated the effects of ER stress-inducing agents that prevent disulfide bond formation (DTT), ER-associated degradation (MG132), or *N*-glycosylation (tunicamycin) or alter calcium homeostasis (thapsigargin) on LPS-induced iNOS expression. After cells were incubated with LPS in the presence or absence of SubAB, mSubAB, or ER stress-inducing agents for 6 h, iNOS expression was analyzed. Although SubAB and ER stress-inducing agents inhibited LPS-induced iNOS expression, mSubAB and vehicle control dimethyl sulfoxide (DMSO) were inactive, suggesting that LPS-induced iNOS expression was inhibited by ER stress (Fig. 2C). We next examined the inhibitory effect of SubAB on LPS-induced iNOS mRNA expression in RAW 264.7 cells. RAW 264.7 cells were treated with LPS for 4 or 24 h in the presence of SubAB or mSubAB, and then total mRNA was used for quantitative PCR analysis. For 4 h of incubation, LPS treatment significantly induced iNOS mRNA expression in RAW 264.7 cells, while SubAB, but not mSubAB, inhibited LPS-induced iNOS mRNA expression (Fig. 2D, left). For 24 h of incubation, SubAB treatment inhibited LPS-induced iNOS mRNA expression, which was slightly increased by mSubAB (Fig. 2D, right). These results indicate that SubAB strongly suppressed LPS-induced iNOS mRNA expression.

SubAB inhibits LPS-induced transcriptional activation of the iNOS promoter in RAW 264.7 cells. In macrophages, LPS-induced iNOS expression is triggered by activation of the Toll-like receptor 4 (TLR4) signaling pathway, followed by binding of transcription factors (i.e., NF-κB, STAT-1, AP-1, C/EBP, CREB, IRF-1, Oct-1) to the iNOS promoter (2, 29, 57). To investigate the effect of SubAB on LPS-induced iNOS promoter activity, RAW 264.7 cells were transiently transfected with mouse iNOS promoter-luciferase reporter plasmid (pGL2-iNOS), and then transcriptional activity was determined by relative luciferase activity 24 h after LPS stimulation in the presence or absence of SubAB or mSubAB. As shown in Fig. 3, LPS treatment significantly increased relative luciferase activity, which was suppressed in the presence of SubAB but not mSubAB. These results indicate that SubAB inhibits LPS-induced transcriptional activation of the iNOS promoter. To determine which sites in the iNOS promoter are responsible for inhibition of iNOS expression by SubAB, we transfected RAW 264.7 cells with iNOS promoter deletion plasmids (see the diagram in Fig. 3). SubAB suppressed LPS-induced luciferase activity of deletion mutants pGL2-iNOS/−724 and pGL2-iNOS/−93. However, inhibitory effects of SubAB on LPS-induced luciferase activity were completely lost in pGL2-iNOS/−40-transfected cells. Stimulatory effects of LPS were also lost in this mutant. These results suggest that the inhibitory effects of SubAB on iNOS promoter activity are contained in the region between −93 bp and −40 bp, which has NF-κB-, NF–IL-6-, and Oct-binding sites (29, 57). To understand the importance of the region for iNOS transcription, RAW 264.7 cells were transfected with pGL2-iNOS full/Δ−46−−203, with a deletion of the region from position −203 to position −46. These cells showed slight LPS-stimulated luciferase activity, suggesting that this region plays an important role in iNOS transcriptional activity in the presence of LPS.

Of note, mSubAB increased the effects of LPS on iNOS transcriptional activity of the intact promoter. This stimulation was not observed in any of the promoter mutants, where, in some instances, slight inhibition was observed.

SubAB inhibits LPS-induced NF-κB nuclear translocation in RAW 264.7 cells. The results of iNOS promoter assays suggested that SubAB affects NF-κB, NF–IL-6, or Oct binding to the iNOS promoter. Since previous studies showed that SubAB inhibited LPS- or TNF-α-induced NF-κB activation through inhibition of IκB-α degradation (17, 37), we examined the effect of SubAB on LPS-induced IκB-α phosphorylation and NF-κB nuclear translocation in RAW 264.7 cells. As shown in Fig. 4A, LPS treatment induced NF-κB p65 and p50 nuclear localization, which was inhibited by pretreatment with SubAB but not mSubAB. In addition, densitometric analysis also showed that SubAB significantly suppressed LPS-induced NF-κB p65 and p50 nuclear localization. NF-κB p65 and p50 subunits most commonly form an NF-κB p65/p50 heterodimer with transactivation activity (10, 50). To confirm the inhibitory effect of SubAB on nuclear translocation of the NF-κB p65/p50 heterodimer, we next performed coimmunoprecipitation with NF-κB p50 antibody in a cytoplasmic fraction from RAW 264.7 cells. In LPS-treated cells, the amount of NF-κB p65/p50 heterodimer was reduced but not in the presence of SubAB. mSubAB did not affect the LPS-induced NF-κB p65/p50 heterodimer. As shown in Fig. 4B, confocal microscopy demon-

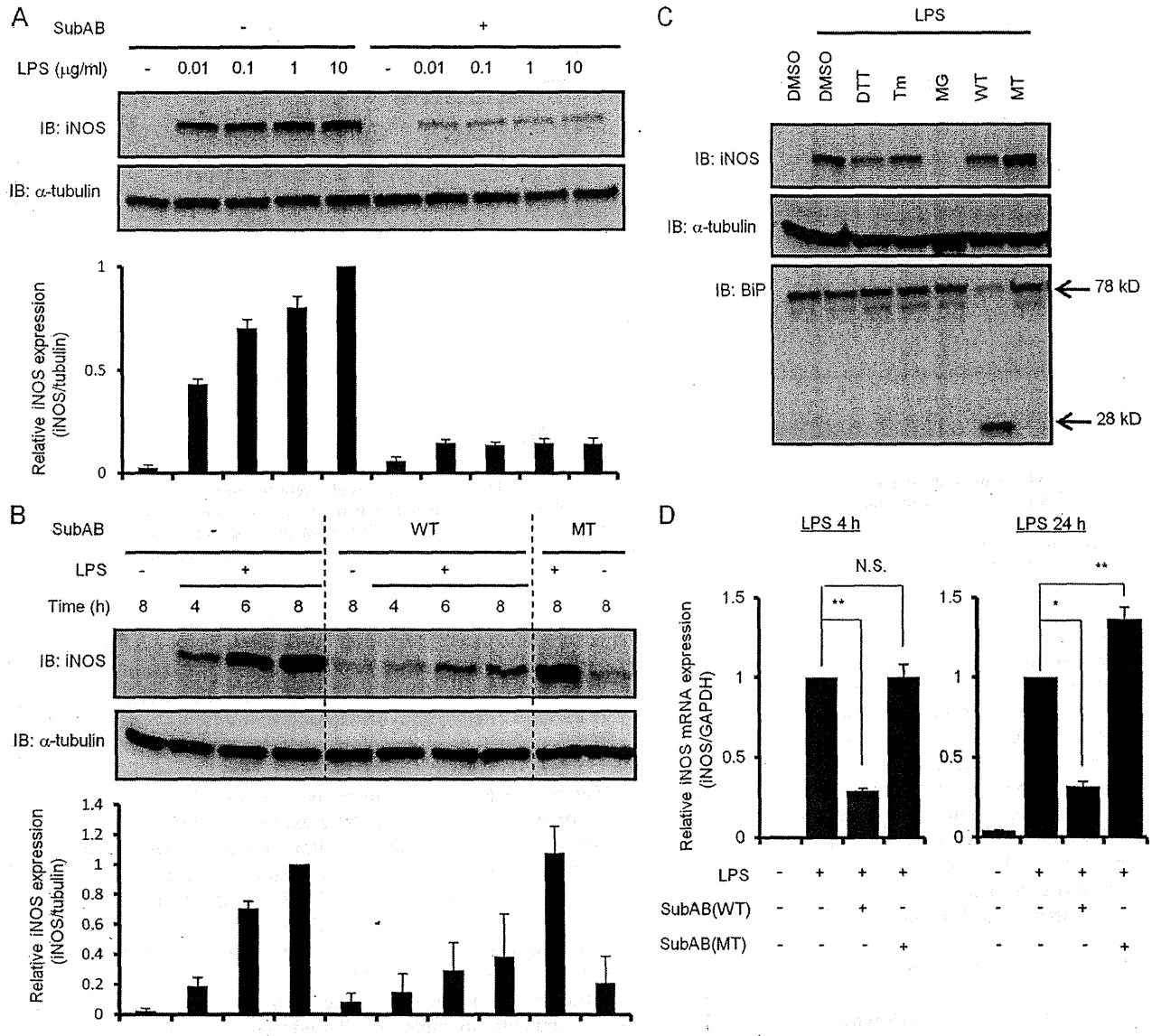

FIG 2 SubAB inhibits LPS-induced iNOS expression by RAW 264.7 cells. (A) RAW 264.7 cells (5×10^4 cells/well) in a 24-well dish were grown in DMEM-1% FBS for 24 h. Cells were treated with LPS (0, 0.01, 0.1, 1, or 10 μg/ml) in the presence or absence of SubAB (0.5 μg/ml) for 24 h. Cell lysates were analyzed by immunoblotting with anti-iNOS or anti-α-tubulin antibodies as a control. Data are representative of at least three separate experiments. (B) RAW 264.7 cells (5×10^4 cells/well) were treated with LPS (10 μg/ml) in the presence or absence of SubAB (WT; 0.5 μg/ml) or mSubAB (MT; 0.5 μg/ml) for the indicated times. Cell lysates were collected from cells and analyzed by immunoblotting as described above. Data are representative of three separate experiments. (C) RAW 264.7 cells (2×10^5 cells/well) were incubated with LPS (10 μg/ml) for 6 h in the presence or absence of DTT (1 mM), tunicamycin (Tm; 1 μg/ml), MG132 (MG; 1 μM), SubAB (WT; 0.5 μg/ml), mSubAB (MT; 0.5 μg/ml), or DMSO as a control. Cell lysates were analyzed by immunoblotting with anti-iNOS, anti-α-tubulin, or anti-BiP/Grp78 antibodies as described above. Data are representative of three separate experiments. (D) RAW 264.7 cells (5×10^4 cells/well) were treated with LPS (10 μg/ml) in the presence or absence of SubAB (WT; 0.5 μg/ml) or mSubAB (MT; 0.5 μg/ml) for 4 or 24 h. Total RNA extracted from the cells was subjected to real-time PCR using specific primers for iNOS as described in Materials and Methods. iNOS expression was normalized to GAPDH (iNOS/GAPDH). Data are means ± SD of values from three separate experiments. Statistical significance: *, $P < 0.01$; **, $P < 0.05$; N.S., not significant.

strated that the NF-κB p65/p50 heterodimer was localized in cytoplasm in untreated RAW 264.7 cells. In LPS-treated cells, the NF-κB p65/p50 heterodimer was translocated into nuclei, while treatment with SubAB, but not mSubAB, blocked the translocation to the nuclei. These data suggest that SubAB inhibits LPS-induced nuclear translocation of the NF-κB p65/p50 heterodimer.

To determine the inhibitory effect of SubAB on the LPS-induced DNA-binding activity of NF-κB, RAW 264.7 cells were transiently transfected with the HIV-3×-κB luciferase reporter construct, which contains a consensus sequence for NF-κB binding, and then LPS-induced transcriptional activity was determined by relative luciferase activity at 4, 8, and 24 h in the presence or absence of SubAB or mSubAB. LPS treatment gradually increased NF-κB-mediated luciferase activity in a time-dependent manner, which was significantly suppressed in the presence of SubAB at 8 or 24 h (Fig. 4C).

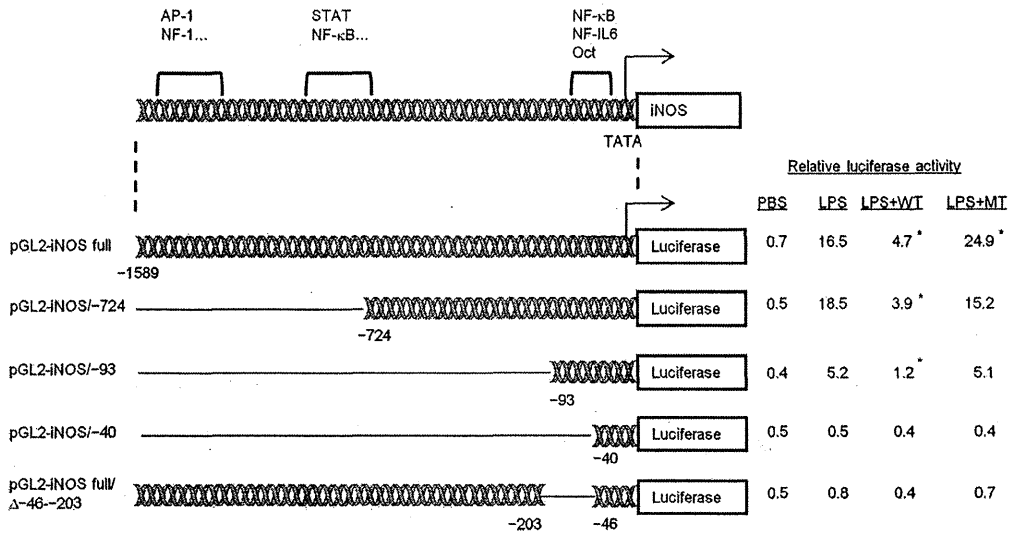

FIG 3 SubAB inhibits LPS-induced iNOS promoter activity in RAW 264.7 cells. RAW 264.7 cells (2.5×10^4 cells/well) were cotransfected with 0.5 μg of pGL2-iNOS and 20 ng of phRL-TK as an internal control. After transfection, cells were incubated with LPS (10 μg/ml) in the presence or absence of SubAB (WT; 0.5 μg/ml) or mSubAB (MT; 0.5 μg/ml) for 24 h. Relative changes in luciferase expression were measured as described in Materials and Methods. Luciferase activity was normalized for *Renilla* luciferase activity. Data are means ± SD of values from three independent assays in triplicate experiments. Statistical significance: *, $P < 0.05$ versus LPS treatment.

To examine whether SubAB affects IκB-α phosphorylation as a trigger of IκB-α degradation, we next investigated IκB-α phosphorylation by immunoblotting. LPS treatment of RAW 264.7 cells increased phosphorylation of IκB-α within 1 h, with a subsequent decrease by 3 h. In the presence of SubAB, BiP cleavage was observed after 30 min of incubation, followed by suppression of LPS-induced IκB-α phosphorylation. A densitometric analysis also showed that SubAB significantly suppressed LPS-induced IκB-α phosphorylation at 0.5 and 1 h. In contrast, mSubAB treatment did not affect LPS-induced IκB-α phosphorylation (Fig. 4D). These results suggest that SubAB suppresses LPS-induced NF-κB nuclear localization through inhibition of phosphorylation-induced IκB-α degradation.

SubAB inhibits LPS-induced NF-κB binding to the iNOS promoter in RAW 264.7 cells. The NF-κB p65/p50 heterodimer has been shown to bind to the NF-κB binding site at a position from −85 to −76 adjacent to the TATA box of the iNOS promoter, which was designated the NF-κBd site (56). To examine whether SubAB treatment suppresses LPS-induced NF-κB p65/p50 heterodimer binding to the NF-κBd site of the iNOS promoter, we performed ChIP-qPCR assay in RAW 264.7 cells using anti-p65 or anti-p50 antibodies. As shown in Fig. 5, LPS treatment dramatically increased p65 and p50 binding to the NF-κBd site. Consistent with the NF-κB reporter assay, SubAB treatment downregulated LPS-induced NF-κB p65/p50 heterodimer binding to the NF-κBd site, whereas mSubAB induced additional binding. Our findings indicate that SubAB treatment suppresses LPS-induced iNOS expression in RAW 264.7 cells via inhibition of NF-κB p65/p50 heterodimer binding to the NF-κBd site in the iNOS promoter; in contrast, mSubAB increases binding.

NF-κB p65/p50 heterodimer is involved in SubAB-mediated inhibition of LPS-induced iNOS expression. To further determine the role of NF-κB p65/p50 heterodimer in LPS-induced iNOS expression, we prepared bone marrow macrophages (BMMs) from wild-type or NF-κB1$^{-/-}$ mice and examined the effect of SubAB on LPS-induced NO production and iNOS expression. First, we evaluated SubAB-mediated inhibition of LPS-induced NO production in BMMs by Griess assay. Compared with RAW 264.7 cells, SubAB treatment more effectively inhibited LPS-induced NO production by BMMs (Fig. 6A). To further investigate an involvement of p50 in SubAB-mediated inhibition of LPS-induced iNOS expression, we next examined the inhibitory effect of SubAB treatment on iNOS expression in wild-type and NF-κB1$^{-/-}$ BMMs by immunoblotting. We first confirmed p50 deficiency in NF-κB1$^{-/-}$ BMMs and the same expression levels of endogenous p65 in wild-type and NF-κB1$^{-/-}$ BMMs (Fig. 6B). As shown in Fig. 6C, LPS-induced iNOS expression in NF-κB1$^{-/-}$ BMMs was slightly attenuated in comparison with wild-type BMMs after 8 h of incubation but not after 24 h of incubation. In addition, densitometric analysis showed that, in wild-type BMMs, SubAB dramatically inhibited LPS-induced iNOS expression by 77% after 8 h of incubation and 95% after 24 h of incubation. On the other hand, SubAB inhibition of LPS-induced iNOS expression in NF-κB1$^{-/-}$ BMMs at 8 and 24 h was significantly decreased at 59% and 71%, respectively. Wild-type BMMs were significantly more responsive for SubAB-mediated inhibition of LPS-induced iNOS expression than NF-κB1$^{-/-}$ BMMs at 8 h and 24 h ($P < 0.01$ and $P < 0.01$, respectively). These results suggest that effects of the NF-κB p50 subunit are partially responsible for SubAB-mediated inhibition of LPS-induced iNOS expression.

SubAB contributes to *E. coli* survival in RAW 264.7 cells. The ability of NO to kill microbes makes it an important part of primordial host defense. Because we found that SubAB inhibited LPS-induced NO production by macrophages, we hypothesized that SubAB contributes to the viability of *E. coli* in macrophages. Therefore, to investigate the effect of SubAB on *E. coli* survival in macrophages, RAW 264.7 cells were infected with a nonpathogenic *E. coli* strain, BL21(DE3), carrying pET23b in the presence or absence of an NOS inhibitor (L-NAME) and purified SubAB or mSubAB, and then bacteria in RAW 264.7 cells were quantified at

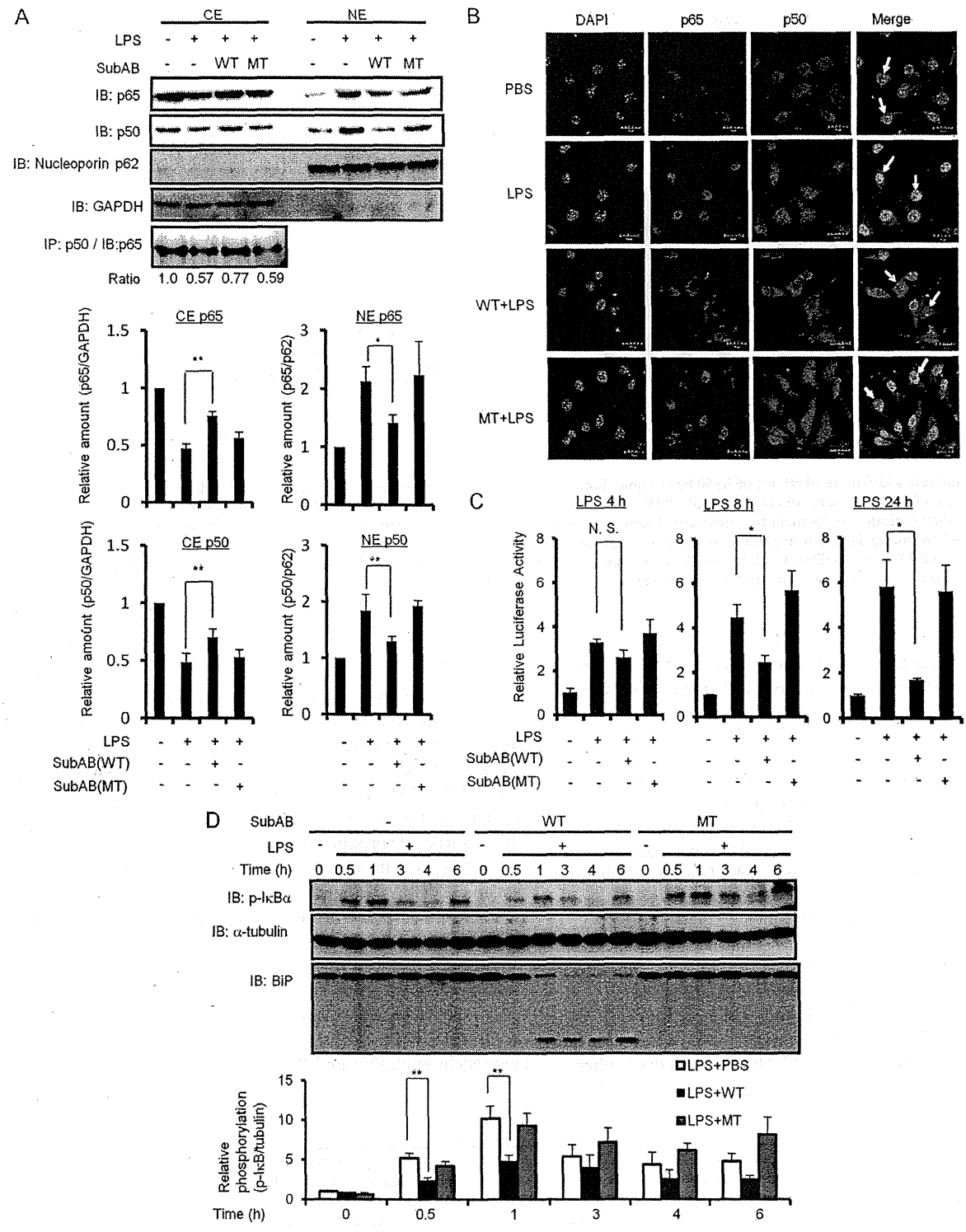

FIG 4 SubAB inhibits LPS-induced NF-κB nuclear translocation in RAW 264.7 cells. (A) After RAW 264.7 cells (5×10^6 cells/dish) were treated with SubAB (0.5 μg/ml) or mSubAB (MT; 0.5 μg/ml) for 3 h in the presence of polymyxin B (10 μg/ml), cells were treated with LPS (10 μg/ml) for 30 min. Cells were collected and lysed in lysis buffer, and cytoplasmic extracts (CE) and nuclear protein extracts (NE) were prepared as described in Materials and Methods. Proteins in CE or NE were analyzed by immunoblotting using anti-NF-κB p65, anti-NF-κB p50, anti-nucleoporin p62 (nuclear protein control), and anti-GAPDH (cytoplasmic protein control) antibodies. Nuclear translocation of p65 and p50 was normalized to nucleoporin p62. CE were immunoprecipitated with anti-NF-κB p50 monoclonal antibody and subjected to analysis by immunoblotting using anti-NF-κB p65 polyclonal antibodies. The relative amounts of p65 and p50 are based on densitometric quantification. Data are means ± SD of values from three independent experiments. Statistical significance: *, $P < 0.01$; **, $P < 0.05$. (B) After RAW 264.7 cells were treated with SubAB (0.5 μg/ml) or mSubAB (MT; 0.5 μg/ml) for 3 h in the presence of polymyxin B (10 μg/ml), cells were treated with LPS